NASA TECHNICAL MEMORANDUM

NASA TM X-2983

NASA TM X-2983

FLIGHT INVESTIGATION OF INSTALLATION EFFECTS ON A PLUG NOZZLE WITH A SERIES OF BOATTAILED PRIMARY SHROUDS INSTALLED ON AN UNDERWING NACELLE

by Verlon L. Head

Lewis Research Center
Cleveland, Ohio 44135

NATIONAL AERONAUTICS AND SPACE ADMINISTRATION • WASHINGTON, D. C. • FEBRUARY 1974

1. Report No.	2. Government Accession No.	3. Recipient's Catalog No.
NASA TM X-2983		

4. Title and Subtitle	5. Report Date
FLIGHT INVESTIGATION OF INSTALLATION EFFECTS ON A PLUG NOZZLE WITH A SERIES OF BOATTAILED PRIMARY SHROUDS INSTALLED ON AN UNDERWING NACELLE	February 1974
	6. Performing Organization Code
7. Author(s)	8. Performing Organization Report No.
Verlon L. Head	E-7612
	10. Work Unit No. 501-24
9. Performing Organization Name and Address	11. Contract or Grant No.
Lewis Research Center National Aeronautics and Space Administration Cleveland, Ohio 44135	
	13. Type of Report and Period Covered
12. Sponsoring Agency Name and Address	Technical Memorandum
National Aeronautics and Space Administration Washington, D. C. 20546	14. Sponsoring Agency Code

15. Supplementary Notes

16. Abstract

Several variations of a boattailed shroud for a 10^{o} conical plug nozzle were tested using an F-106B aircraft for Mach 0.6 to 1.3. The data were obtained so that the tradeoff between boattail and plug size could be studied for an underwing nacelle location. The nozzles were tested with a J85-GE-13 turbojet engine, and the data were compared to previous flight results of installed plug nozzles. Boattail area varied from 31 to 66 percent of the nacelle area. The effect of increasing projected boattail area was to increase the gross thrust coefficient in the same way as from isolated data for flight Mach numbers below 0.85. The highest gross thrust coefficient (0.958) was obtained at Mach 0.95 with a long circular arc shroud configuration with a very small amount of secondary air flow.

17. Key Words (Suggested by Author(s))	18. Distribution Statement
Airframe installation effects; Plug nozzles; Propulsion system; Flight test; Underwing nacelles	Unclassified - unlimited
	Cat.28

19. Security Classif. (of this report)	20. Security Classif. (of this page)	21. No. of Pages	22. Price*
Unclassified	Unclassified	30	$3.00

* For sale by the National Technical Information Service, Springfield, Virginia 22151

FLIGHT INVESTIGATION OF INSTALLATION EFFECTS ON A PLUG NOZZLE WITH A SERIES OF BOATTAILED PRIMARY SHROUDS INSTALLED ON AN UNDERWING NACELLE

by Verlon L. Head

Lewis Research Center

SUMMARY

Four configurations of a boattailed plug nozzle were installed on an underwing nacelle mounted on an F-106B aircraft housing a J85-GE-13 turbojet engine.

The 10^{o} conical plug was tested with four boattailed primary shrouds with various amounts of boattailing upstream of the primary exit. The data were obtained so that the tradeoff between boattail and plug size could be studied for an underwing nacelle location at Mach numbers from 0.6 to 1.3. Boattail area varied from 31 to 66 percent of the nozzle area.

Nozzle thrust performance, pumping characteristics, and the ratio of boattail drag to ideal primary thrust were determined for the altitude Mach number profile. In addition, the effect of nozzle pressure ratio was determined at a subsonic cruise of Mach 0.9. The effect of increasing the projected boattail area was to increase the gross thrust coefficient in the same way as from isolated data for flight Mach numbers below 0.85. At higher flight Mach numbers this trend no longer held because of installation effects. A long circular arc primary shroud (largest boattail area) had the highest gross thrust coefficient of 0.958 at Mach 0.955 and the lowest boattail drag at subsonic Mach numbers up to 0.98. Gross thrust coefficients varied only slightly from Mach 0.7 to 0.9, and boattail drag coefficients were almost constant to Mach 0.9 for all four configurations. The short conical shroud (smallest boattail area) had the highest drag coefficient of the four. All configurations exhibited an increasing thrust coefficient and decreasing drag coefficient with an increasing pressure ratio at Mach 0.9 and exhibited about the same sensitivity for both parameters.

INTRODUCTION

As a continuing part of a current program in airbreathing propulsion, the Lewis Research Center is investigating airframe installation effects on the performance of exhaust nozzle systems appropriate for use at supersonic speeds. In this program, airframe installation effects are being investigated in both wind tunnel and flight tests at off-design and transonic speeds.

Recent experience has shown that nozzle performance can be appreciably affected by installation on an aircraft, especially at off-design conditions (refs. 1 to 8). With an engine nacelle installation typical of supersonic cruise aircraft, the nacelle may be installed close to the lower surface of a large wing with the nozzle extending downstream of the trailing edge. This aft location of the nacelle provides shielding of the inlet by the forward wing surface to minimize angle-of-attack effects and may also provide favorable interference between the nacelle and wing. To investigate the effect of the airframe flow field on nozzle performance for a nacelle location of this type, the Lewis Research Center is conducting a flight test program using a modified F-106B aircraft with underwing engine nacelles. This flight system provides the capability of testing complex nozzles at a larger size than possible in wind tunnels where models are limited to a small size to minimize wall interference effects.

A flight test program was initiated to determine installation effects on large-scale plug nozzle designs, free of model blockage and tunnel wall effects. A plug nozzle with various geometric changes of shroud and primary flap has been previously flight tested (ref. 8) and showed significant differences between isolated wind tunnel results and installed flight test results.

Nacelle maximum diameters are dictated many times by factors other than nozzle pressure ratio such as engine cycle, engine accessory packing, and sometimes installation considerations. When these diameters are considerably larger than desired for the required nozzle exit area, some consideration must be given to the method of accomplishing this with as little loss in performance as possible. With a plug nozzle design one has the choice of using an oversize plug with little or no boattailing against an "on-design" plug with maximum upstream boattailing (ref. 9). In an attempt to define the tradeoffs between these two approaches for an underwing installation, a series of boattailed shrouds with different projected areas and shapes was designed to be tested with the existing J-85 nozzle plug assembly (ref. 8).

Three nozzle shrouds having a circular arc transition from the cylindrical section with a radius of 15.87 centimeters (6.25 in.) followed by a 15° conical boattail were tested. The length of the shortest shroud was limited by an existing shroud attachment flange and the longest by the F-106 takeoff ground clearance considerations. A fourth

shroud, having a circular arc boattail shape with the same length as the long conical shroud, was also tested. In an attempt to minimize the effect of cooling flow on the results, the secondary air flow was discharged through the plug tip with the flow being limited by the existing flow passages through the three plug-support struts. The boattailed shrouds also served as the primary flap. A constant throat area equivalent to the J-85 military operation was maintained for the four shrouds.

The flight results obtained for Mach 0.6 to 1.3 resulted in a pressure ratio range of 2.7 to 5.4 with a nominal corrected secondary air flow ratio of 0.01. The results are presented as gross thrust coefficient, boattail drag coefficient, pumping characteristics, boattail pressure distributions, and comparisons with two nozzle configurations from reference 8.

SYMBOLS

A	cross-sectional area, cm^2 ($in.^2$)
A_n	cross-sectional area of nozzle cylindrical section, 3166.9 cm^2 (490.9 $in.^2$)
$C_{D,\beta}$	axial pressure drag coefficient in direction of nozzle axis, axial force/$q_0 A_n$
c_p	pressure coefficient, $(p - p_0)/q_0$
D	drag in direction of nozzle axis, kN (lbf)
d	diameter, cm (in.)
d_n	diameter of nozzle cylindrical section, 63.5 cm (25 in.)
F	nozzle thrust in direction of nozzle axis, kN (lbf)
h	geopotential pressure altitude, m (ft)
ℓ_β	axial length of boattail from boattail shoulder to primary exit
M	Mach number
P	total pressure, absolute, kN/m^2 (psia)
p	static pressure, absolute, kN/m^2 (psia)
q	dynamic pressure, $0.7\, p_0 M_0^2$, kN/m^2 (psi)
r	radius, cm (in.)
r_β	boattail juncture radius, cm (in.)
T	total temperature, absolute, K (^oR)
W	weight flow, kg/sec (lbm/sec)

x	axial distance from nozzle attachment station, cm (in.)
α_0	aircraft angle of attack, deg
β	angle of boattail surface at trailing edge, deg
δ_e	elevon deflection angle (+down, -up) , deg
τ	ratio of secondary to primary total temperatures, T_s/T_8
ω	ratio of secondary to primary weight flows, W_s/W_8
$\omega\sqrt{\tau}$	corrected secondary weight flow ratio

Subscripts:

e	effective
ip	ideal primary
n	nozzle
s	secondary
se	secondary exit
β	boattail
0	free stream
8	primary exit

APPARATUS AND PROCEDURE

Flight Installation

Flight tests for this research program were conducted with an F-106B aircraft modified to carry two underwing nacelles. The aircraft is shown in flight in figure 1 with a previously tested plug nozzle (ref. 8) and with a reference nozzle used to calibrate the nacelle drag force (ref. 10). The 63.5-centimeter (25-in.) diameter nacelles were located at approximately 32-percent wing semispan, with the exhaust nozzles extending beyond the wing trailing edge. The nacelles had a downward incidence of $4\frac{1}{2}^{\circ}$ (relative to the wing chord) so that the aft portion of the nacelles was tangent to the trailing surface of the wing. More details of the basic aircraft dimensions and nacelle details are given in reference 5. A schematic drawing of the nacelle-engine underwing test installation is shown in figure 2. The nacelle had a normal shock pitot inlet and contained a calibrated J85-GE-13 afterburning turbojet engine. The variable-area nozzle was removed and replaced with a fixed area plug nozzle. Secondary air to

cool the engine was supplied from the inlet through a conical rotating valve located at the periphery of the compressor face. The secondary flow passed through the three plug support struts into the plug and was discharged overboard through the open plug tip.

The nacelle support system consisted of a front and rear link with a load-cell assembly between the links. The nacelle axial force was transmitted to the wing through the load cell, whose axis was parallel to that of the nacelle. An accelerometer in the nacelle was used to compensate the load cell for axial acceleration. The axial force transmitted to the compensated load cell can be divided into two parts: (1) nacelle drag forward of the research nozzle, referred to as the tare force, and (2) research-nozzle gross thrust minus drag. The tare force was determined from previous research test data which was obtained by using a calibrated cylindrical ejector nozzle (ref. 10). The research-nozzle gross thrust minus the drag was determined by adding the tare force to the compensated load-cell measurement.

Boattail Plug Nozzle

A side view of the intermediate length conical shroud configuration showing its installation relative to the trailing edge of the wing and elevon is given in figure 3. Figure 4 shows the long conical shroud configuration installed on the aircraft, and figure 5 shows an aft view of the same shroud plus a view of the secondary flow opening in the plug tip. The basic plug body (fig. 6) was a 10° half-angle conic structure which was attached to the nacelle by three equally spaced support struts. A section of the strut outside the primary flow passage was removed to allow secondary cooling air to be routed overboard through the plug tip (see fig. 2). A restriction to military or part power operation was imposed so as not to exceed the plug design temperature of 1006 K (1810° R), thereby eliminating any nozzle cooling requirements. The primary exit area was sized to give an effective exit area of approximately 710 square centimeters (110 in.^{2}) so that the engine could attain a military power setting.

Four boattailed primary shrouds were designed to fit an existing plug nozzle (ref. 8) with minor modifications. Three of the boattailed primary shrouds were 15° conical surfaces with a circular arc radius transition to the cylindrical section of 15.87 centimeters (6.25 in., $r_\beta/d_n = 0.25$). The fourth shroud had an all circular arc boattail with a radius of 291.26 centimeters (114.67 in., $r_\beta/d_n = 4.58$). Other dimensional characteristics are shown in figure 6, and table I gives a number of additional nozzle variables.

Instrumentation

Instrumentation for the nozzle configurations was limited to boattail static pressures and secondary flow instrumentation, which consisted of total and static pressure and total temperature. Shown in figure 7 are the locations of the boattail statics and secondary temperatures and pressures. The long conical primary shroud used fifty static pressures in ten rows, while the remaining three shrouds had only twenty statics in four rows (fig. 7). All the shrouds had one static pressure upstream of the boattail surface at 0°, 30°, 225°, and 270°. The instrumentation for measuring secondary cooling flow was located inside the plug tip in a 5.08-centimeter- (2-in.-) long cylindrical section just upstream of the secondary exit. This measuring station consisted of two total pressures, two total temperatures, and four static pressures.

An onboard digital data system was used to record the pressures and temperatures on magnetic tape. A flight-calibrated test boom located on the aircraft nose was used to determine the free-stream static and total pressures, aircraft angle of attack, and yaw angle.

Procedure

Performance characteristics of the plug nozzle were obtained over flight Mach numbers from 0.6 to 1.3 and at Reynolds numbers that varied from 8.5×10^{6} per meter (2.6×10^{6} /ft) at Mach 0.6 to 14×10^{6} per meter (4.4×10^{6} /ft) at Mach 1.3. Flying the aircraft at the nominal altitude Mach number profile shown in figure 8(a) resulted in the angles of attack and elevon deflections shown in figure 8(b). The exhaust nozzle pressure ratio schedule for the four configurations is given in figure 8(c) as a function of Mach number.

Data Reduction

Engine airflow was determined by using the calibration results from reference 10 and by measuring engine speed, total pressure, and total temperature at the compressor face. Fuel flow was obtained from a calibrated flowmeter. Total temperature T_8, total pressure P_8, and effective area $A_{e,8}$ were obtained by using the values of engine airflow and fuel flow, measured values of total pressure and temperature at the turbine discharge (station 5), and afterburner pressure drop calibration results from reference 11.

The gross thrust coefficient is defined as nozzle gross thrust minus drag divided by the ideal thrust of the primary stream - $(F-D)/F_{ip}$. The ideal thrust of the primary stream was determined from the calculated primary mass flow expanded isentropically from its value of total pressure and temperature at station 8 (primary exit) to ambient pressure. The research nozzle thrust minus drag was determined by adding the tare force to the compensated load-cell measurement (ref. 10). The boattail drag coefficient for the four nozzle configurations was computed as follows:

$$C_{D,\beta} = -\frac{1}{A_n}\sum_{i=1}^{n} C_{p,i} A_i$$

where $C_{p,i}$ is the local boattail pressure coefficient and A_i is the projected area assigned to the i^{th} orifice. The five orifices in each row were located such that an equal projected area was assigned to each orifice. For the long conical shroud which had ten rows of statics, the 0^o, 30^o, 60^o, 300^o, and 330^o rows were averaged, and they represented 41.67 percent of the total area. The rows at 135^o, 180^o, and 225^o represented 37.5 percent, and the remaining rows at 90^o and 270^o represented 20.83 percent of the total area. The short conical, intermediate conical, and long circular arc boattailed configurations had only four rows of five statics each at 0^o, 30^o, 225^o, and 270^o with each row representing 16.61, 31.31, 33.23, and 18.85 percent of the boattail area, respectively.

RESULTS AND DISCUSSION

Nozzle Thrust Performance and Comparisons

The flight performance data for the four boattailed primary shroud configurations are shown in figure 9. The performance for both the short and intermediate conical shrouds were almost identical for the entire Mach number profile. For these two configurations the nozzle gross thrust coefficient was 0.907 at Mach 0.7 and increased to a peak of 0.934 at Mach 0.86. The performance dropped off between Mach 0.86 and 0.95 to a value of about 0.90 at Mach 0.9 and then reached another peak of 0.928 at Mach 0.95. As the Mach number increased, the performance dropped off to its minimum

value of 0.78 at Mach 0.975; at higher Mach numbers, the performance increased slightly.

The long conical and long circular arc boattail shroud configurations gave performance results which were about equal for Mach numbers up to 0.87. The gross thrust coefficients for the long conical and long circular arc shrouds at Mach 0.86 were 0.945 and 0.950 and at Mach 0.95 were 0.928 and 0.958. Of the four configurations, the long conical shroud had the lowest gross thrust coefficient, which was 0.745, near Mach 1.0; the highest was 0.806 for the long circular arc shroud.

The flight performance data for the short and intermediate conical boattailed nozzles are compared with the results obtained from a previous flight test program (ref. 8) for plug nozzles. The compared results are shown in figures 10 and 11. The short conical shroud boattailed configuration is compared to the cylindrical nacelle plug nozzle, which had a fully retracted shroud and a 17° conical primary flap. It is shown in figure 10 how the two plug nozzle configurations compare at Mach 0.8, 0.85, 0.90, and 0.95. The short conical boattailed nozzle had from 1 to 2 percent higher thrust coefficients at Mach 0.80 and 0.85 and about 1 percent lower for Mach 0.90 and 0.95 than the cylindrical nacelle plug extrapolated for a corrected secondary weight flow of about 0.01. The cylindrical nacelle plug nozzle had the same ratio of primary exit to nacelle diameter ratio as the short conical configuration of this report. The same is also true for the intermediate conical boattail configuration and the boattailed nacelle plug nozzle (ref. 8), which are compared in figure 11. The intermediate conical boattailed nozzle had the same gross thrust coefficient at Mach 0.8 and 0.90, about 1 percent lower at Mach 0.82, and 2.5 percent lower at Mach 0.95 as shown in figure 11.

The effect of boattail projected area on gross thrust coefficient for Mach 0.8 and 0.9 is shown in figure 12. The results from this test show the same sensitivity as did the isolated wind tunnel results in reference 12. Generally, the thrust coefficient increases with increasing boattail area and decreasing plug area for low pressure ratios, but there can be an installation effect which can change this trend. For this test the gross thrust coefficient for the long conical boattail configuration ($A_{\beta}/A_n = 0.667$) had a lower value than the intermediate boattail ($A_{\beta}/A_n = 0.49$) at Mach 0.9. This was because the performance of the nozzle is sensitive to the boattail shoulder location for this type of nozzle installation (ref. 6) from Mach 0.85 to 0.97. The long conical boattail configuration had its boattail shoulder located farthest aft for the four configurations tested. At Mach 0.8 where the boattail shoulder location has very little effect, the gross thrust coefficient fell in line with the isolated data trend. The reason for the difference in performance level between the trend indicated by isolated data and flight data is because of plug geometry and boattail geometry differences. The boattails for the data of

reference 12 were all circular arcs, whereas the boattail configurations for this report were conical, except for one, which resulted in a larger pressure drag. Another reason for lower thrust coefficients was that the larger diameter plug upstream of the throat resulted in a higher friction drag on the plug compared to the configurations in reference 12. If a minimum-size plug had been used for each configuration with all circular arc boattails, the results should have been approximately the same as that of reference 12.

Boattail Drag

The effect of the boattailed primary shroud geometry on the boattail drag coefficient for the four shroud configurations is shown in figure 13 for Mach 0.6 to 1.3. The short conical configuration had the highest drag coefficient up to Mach 0.975, but it had the lowest at higher Mach numbers. The long conical configuration had the lowest drag coefficient up to Mach 0.875, but above Mach 0.98 it had the highest. The intermediate conical and long circular arc configurations had drag coefficients which fell between the short and long conical shroud configurations. The intermediate was a little higher than the circular arc shroud up to Mach 1.0, and both were about equal at higher Mach numbers. All four configurations had essentially a constant value of drag coefficient up to Mach 0.9 where there is a decrease to their minimum value near Mach 0.94. Near Mach 0.94 the drag rise begins and reaches a peak at about Mach 0.98 where the drag coefficient then decreases with increasing Mach numbers.

Figure 14 shows the effect of boattail geometry on the ratio of boattail drag to ideal thrust of the primary flow. The trends, of course, are the same as for the drag coefficient since the ideal primary thrust is approximately the same at each Mach number for all four nozzle configurations. There is only a 2-percent difference between the lowest and highest values up to Mach 0.93, but much greater at higher Mach numbers.

Subsonic Cruise Thrust and Drag Characteristics

The effect of nozzle pressure ratio on nozzle gross thrust coefficient and boattailed primary shroud drag ratio for a subsonic cruise Mach number of 0.9 is shown in figure 15. These data were obtained for a pressure ratio range of 2.2 to 3.7. All four configurations exhibited an increasing value of thrust coefficient with increasing pressure ratio, and all configurations had about the same sensitivity, which was also about the same as the boattailed nacelle plug nozzle (ref. 8).

Figure 15 also shows how the ratio of shroud boattail drag to primary thrust is affected by changes in nozzle pressure ratio. It can be seen in the figure that the drag ratio becomes less as the pressure ratio increases for all four configurations, and they all had about the same sensitivity to nozzle pressure ratio. At a pressure ratio of 3.6, the short conical shroud had the highest drag ratio and the long circular arc had the lowest.

Pumping Characteristics

The nozzle pumping characteristics for the nominal flight profile are shown in figure 16 for the four nozzle configurations tested. Shown in the figure are the corrected secondary weight flow and the ratio of secondary exit total pressure to primary total pressure. The amount of secondary flow was limited because of the restricted air passageway through the plug struts and the plug tip exit area of 36.84 square centimeters (5.71 in.^{2}). The corrected secondary flow varied from 0.005 to 0.015 over the Mach number range of 0.6 to 1.3. Because of the small secondary flow area, the ratio of total pressure at the secondary flow exit to the primary total pressure was quite high.

The effect of nozzle pressure ratio on its pumping characteristics at a flight Mach number of 0.9 is shown in figure 17. There was very little change in corrected secondary flow with nozzle pressure ratio for the short and intermediate shroud configurations. Also, the secondary pressure ratio varied directly with primary total pressure (secondary total pressure not affected by primary total pressure). With the long conical and long circular arc shroud configurations, the primary pressure ratio began to have a considerable effect on corrected secondary air flow at pressure ratios of 3.0 and greater. With the long shroud length reducing the amount of plug surface downstream of the primary exit, the static pressure around the secondary exit was increased by the primary jet for pressure ratios above 3.0, which resulted in a decrease in corrected secondary flow.

Boattailed Shroud Pressure Distributions

The effect of nozzle installation on the boattailed shroud pressure distributions is shown in figure 18 for the four configurations at four Mach numbers from 0.85 to 1.04. As seen from previous data (refs. 5, 6, and 8), there is a large circumferential static pressure variation over almost the entire length of the boattail and especially just downstream of the boattail shoulder. The short conical shroud exhibited the largest

variation in static pressure distribution as well as the lowest average pressure coefficient. The long circular arc boattailed shroud exhibited the least variation in pressure distribution and the highest average pressure coefficient.

SUMMARY OF RESULTS

A flight test program was conducted to study the installation effect on a 10^{o} conical plug nozzle with various geometric changes of a boattailed primary shroud. These geometric changes were designed to have various amounts of upstream boattailing so that the trade-off between upstream boattailing and plug size could be studied for an underwing nacelle location at Mach numbers from 0.6 to 1.3. The primary throat area was fixed equal to the military area for the J85-GE-13 engine ($A_{e,8}$ = 710 cm^2 (110 $in.^2$)). The following results were obtained:

1. The effect of increasing the projected boattail area is to increase the gross thrust coefficient at subsonic Mach numbers and low pressure ratios. The sensitivity of this effect was the same as from isolated wind tunnel tests for flight Mach numbers below 0.85. At higher flight Mach numbers this trend no longer held because of installation effects.

2. The nozzle with the long circular arc primary and largest projected boattail area had the highest gross thrust coefficient of the four configurations over the entire Mach number range tested. It had a peak of 0.958 at Mach 0.955.

3. Above Mach 0.86, all four configurations exhibited an abrupt dip in performance, reaching a minimum at Mach 0.9. The performance then rises again until approximately Mach 0.96, where the drag rise starts.

4. A comparison of the short conical shroud configuration with a cylindrical nacelle plug nozzle shows the short conical configuration to have a higher gross thrust coefficient below Mach 0.9. The largest difference is 2 percent at Mach 0.85.

5. A comparison of thrust coefficients of the intermediate conical shroud configuration with a similar boattailed nacelle plug nozzle shows it to be the same at Mach 0.9 and below, but 2.5 percent lower at Mach 0.95.

6. Boattail drag coefficients were almost constant up to Mach 0.9 for all four shroud configurations with the short conical one having the highest. The same holds true for the ratio of boattail drag to ideal primary thrust.

7. At Mach 0.9 all configurations exhibited an increasing thrust coefficient with increasing pressure ratio and each configuration had about the same sensitivity.

Lewis Research Center,
National Aeronautics and Space Administration,
Cleveland, Ohio, October 2, 1973,
501-24.

REFERENCES

1. Greathouse, William K.: Blending Propulsion with Airframe. Space/Aeronautics, vol. 50, no. 6, Nov. 1968, pp. 59-68.
2. Corson, Blake W., Jr.; and Runckel, Jack F.: Exploratory Studies of Aircraft Afterbody and Exhaust-Nozzle Interaction. NASA TM X-1925, 1969.
3. Schnell, W. C.; and Migdal, D.: An Experimental Evaluation of Exhaust Nozzle/Airframe Interference. J. Aircraft, vol. 7, no. 5, Sept.-Oct. 1970, pp. 396-400.
4. Blaha, Bernard J.; and Mikkelson, Daniel C.: Wind Tunnel Investigation of Airframe Installation Effects on Underwing Engine Nacelles at Mach Numbers from 0.56 to 1.46. NASA TM-1683, 1968.
5. Mikkelson, Daniel C.; and Head, Verlon L.: Flight Investigation of Airframe Installation Effects on a Variable Flap Ejector Nozzle of an Underwing Engine Nacelle at Mach Numbers from 0.5 to 1.3. NASA TM X-2010, 1970.
6. Head, Verlon L.: Flight Investigation of an Underwing Nacelle Installation of Three Variable-Flap Ejector Nozzles. NASA TM X-2478, 1972.
7. Head, Verlon L.: Flight Investigation of an Underwing Nacelle Installation of an Auxiliary-Inlet Ejector Nozzle with a Clamshell Flow Diverter from Mach 0.6 to 1.3. NASA TM X-2655, 1972.
8. Samanich, Nick E.; and Chamberlin, Roger: Flight Investigation of Installation Effects on a Plug Nozzle Installed on an Underwing Nacelle. NASA TM X-2295, 1971.
9. Rabone, George R.: Low Angle Plug Nozzle Performance Characteristics. Paper 66-664, AIAA, June 1966.
10. Groth, Harold W.; Samanich, Nick E.; and Blumenthal, Philip Z.: Inflight Thrust Measuring System for Underwing Nacelles Installed on a Modified F-106 Aircraft. NASA TM X-2356, 1971.

11. Antl, Robert J.; and Burley, Richard R.: Steady-State Airflow and Afterburning Performance Characteristics of Four J85-GE-13 Turbojet Engines. NASA TM X-1742, 1969.
12. Harrington, Douglas E.: Performance of Convergent and Plug Nozzles at Mach Numbers from 0 to 1.97. NASA TM X-2112, 1970.

TABLE I. - NOZZLE VARIABLES

Primary shroud configuration	Ratio of effective throat area to nozzle area, $A_{e,8}/A_\eta$	Boattail projected area to nozzle area, A_β/A_η	Boattail trailing-edge angle, β, deg	Boattail length to nozzle diameter, l_β/d_η	Boattail-juncture radius of curvature to nozzle diameter ratio, r_β/d_η
Short conical	0.22	0.313	15	0.354	0.25
Intermediate conical	.22	.490	15	.568	.25
Long conical	.22	.667	15	.785	.25
Long circular arc	.22	.667	17.5	1.379	4.58

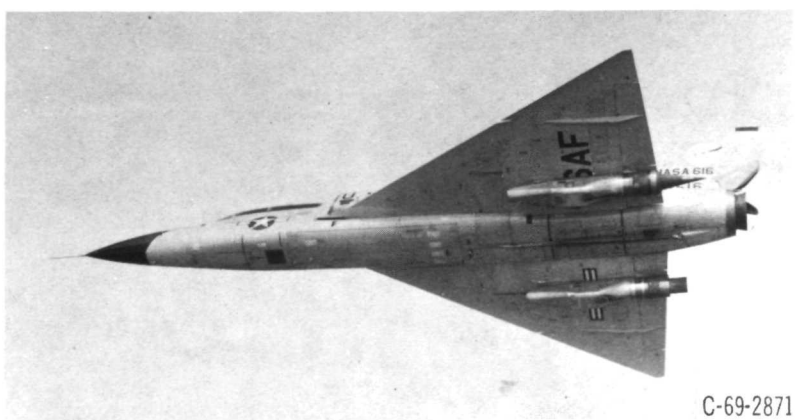

Figure 1. - Modified F-106B aircraft in flight.

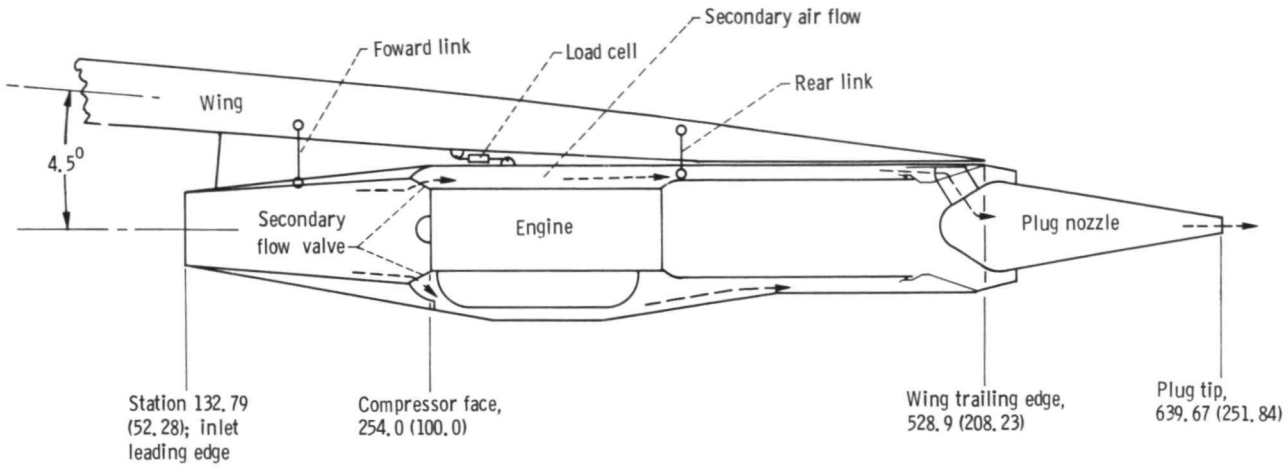

Figure 2. - Schematic of test installation. All dimensions are in centimeters (in.).

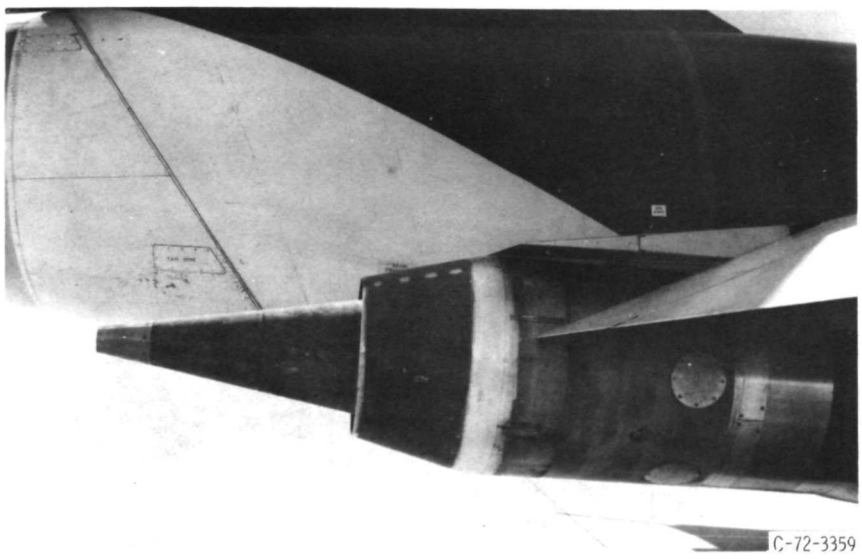

Figure 3. - Intermediate length conical shroud.

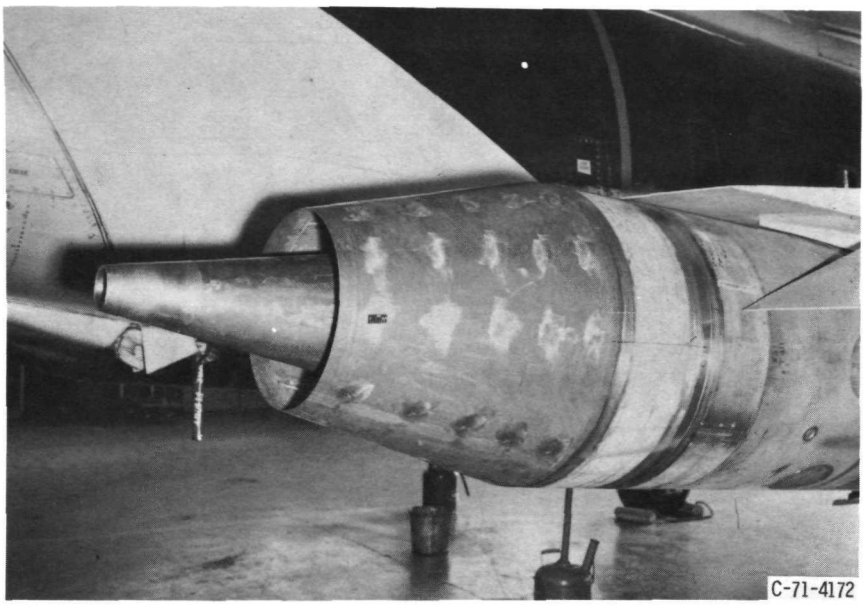

Figure 4. - Long conical shroud.

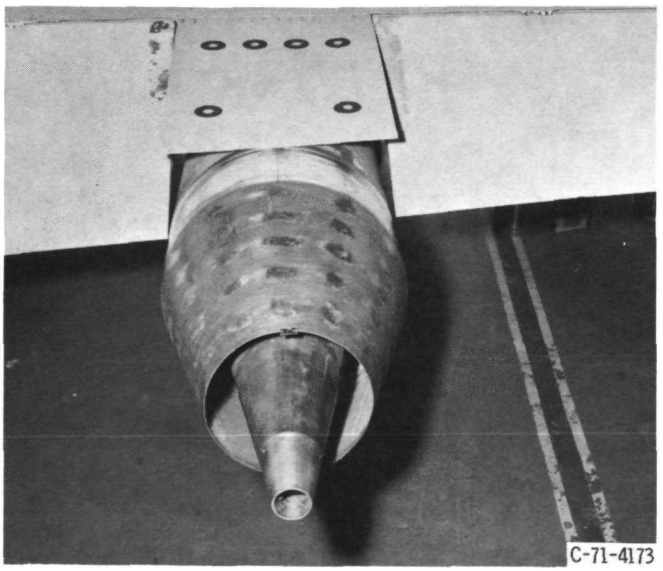

Figure 5. - Aft view of plug nozzle showing secondary flow opening in plug tip. Shown is long conical shroud.

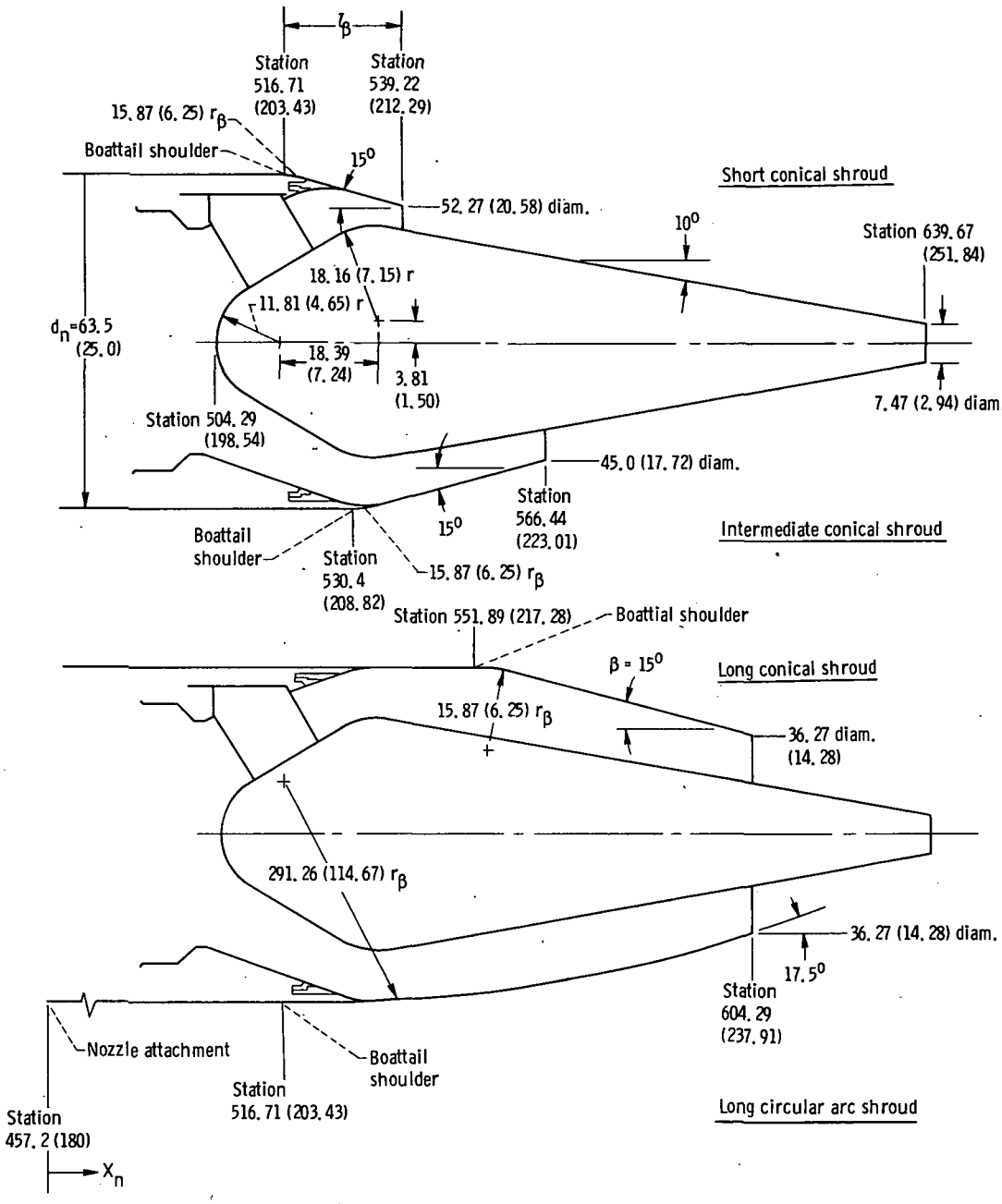

Figure 6. - Nozzle dimensions. All dimensions are in centimeters (in.).

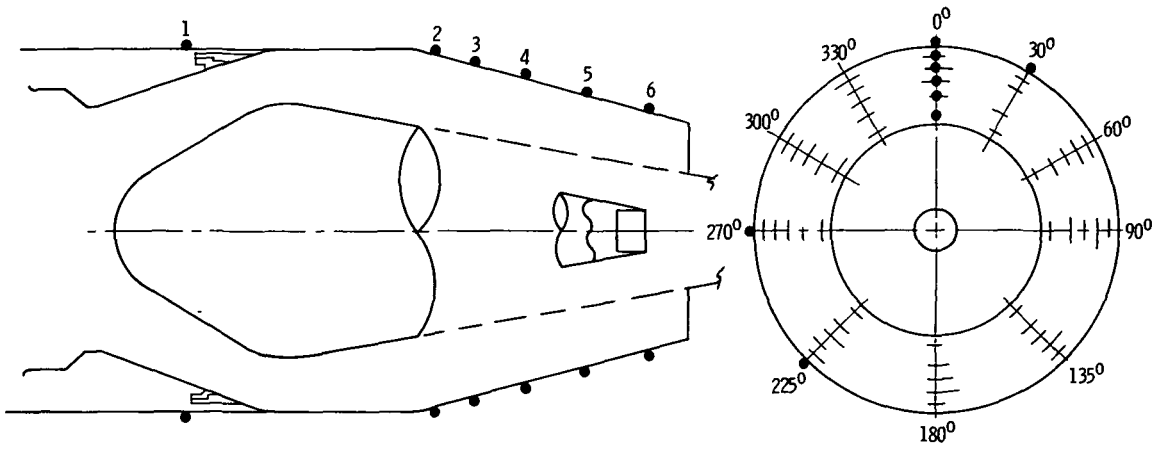

Location	Orifice location	Nozzle shroud configuration							
		Short conical[a]		Intermediate conical[a]		Long conical		Long circular arc	
		Nozzle station							
		cm	in.	cm	in.	cm	in.	cm	in.
Clyindrical section	1	516.64	203.40	516.64	203.40	516.64	203.40	516.64	203.40
Boattail	2	520.06	204.75	534.39	210.39	558.09	219.72	539.47	212.39
	3	524.03	206.31	540.74	212.89	566.60	223.07	557.15	219.35
	4	528.22	207.96	547.45	215.53	575.84	226.71	571.42	224.97
	5	532.49	209.64	554.61	218.35	586.10	230.75	586.15	230.77
	6	537.01	211.42	562.38	221.41	597.74	235.33	597.97	235.42

[a]These configurations have only four rows of boattail instrumentation at circumferential positions of 0°, 30°, 225°, and 270°.

(a) External surface pressure instrumentation.

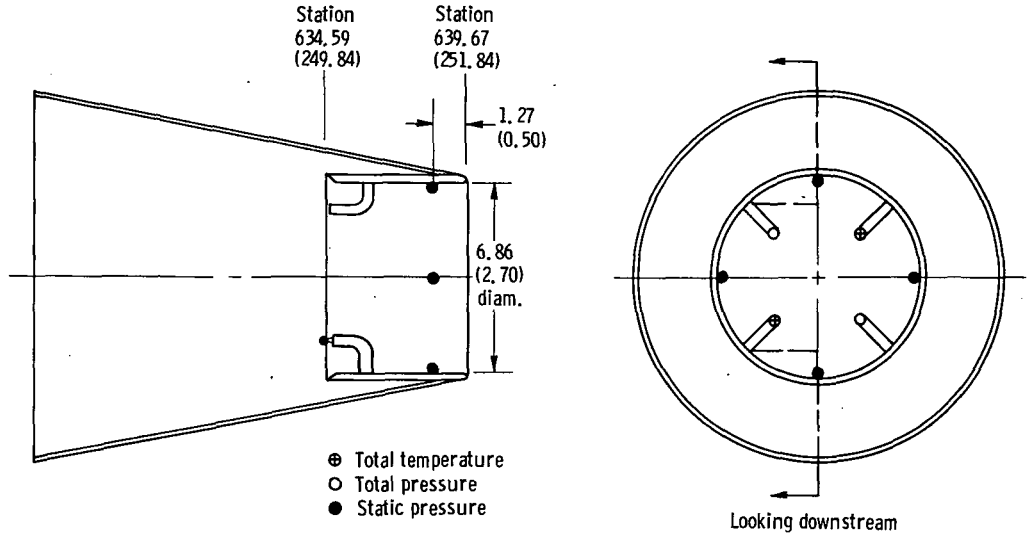

(b) Secondary flow instrumentation.

Figure 7. - Plug nozzle instrumentation. All dimensions are in centimeters (in.).

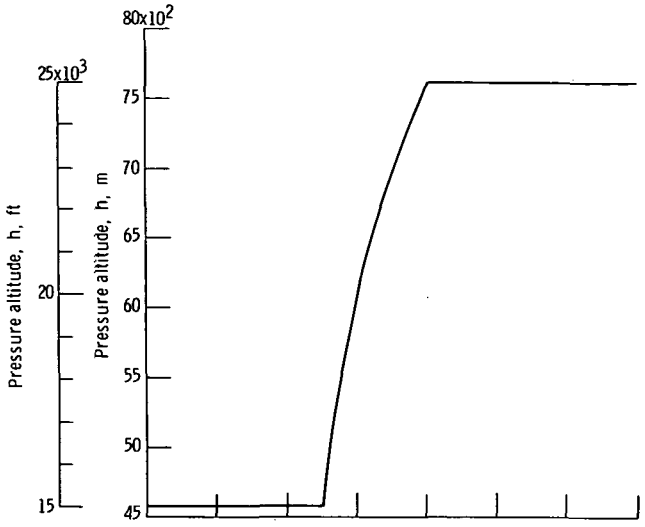

(a) Nominal flight test altitude Mach number profile.

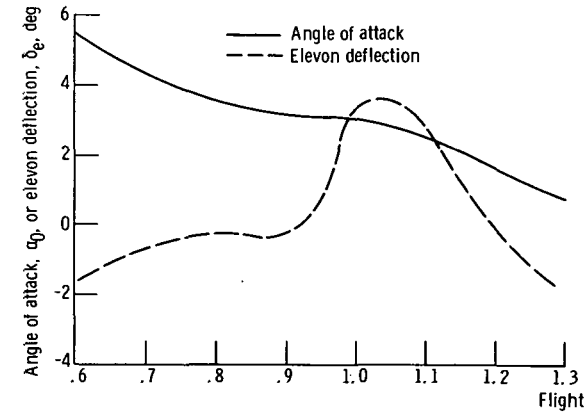

(b) Nominal angle of attack and elevon deflection with nacelles installed.

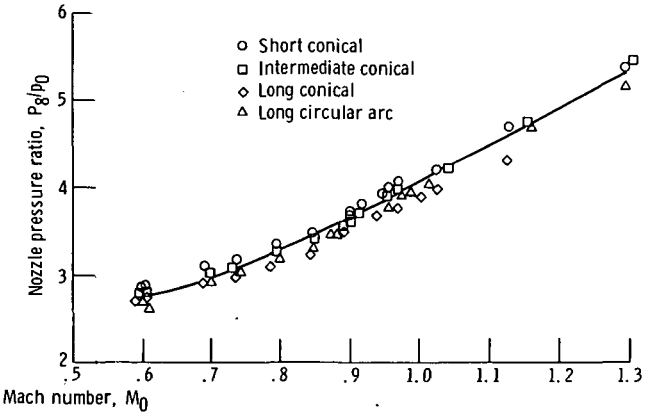

(c) Nozzle pressure ratio, military power setting.

Figure 8. - Flight test conditions.

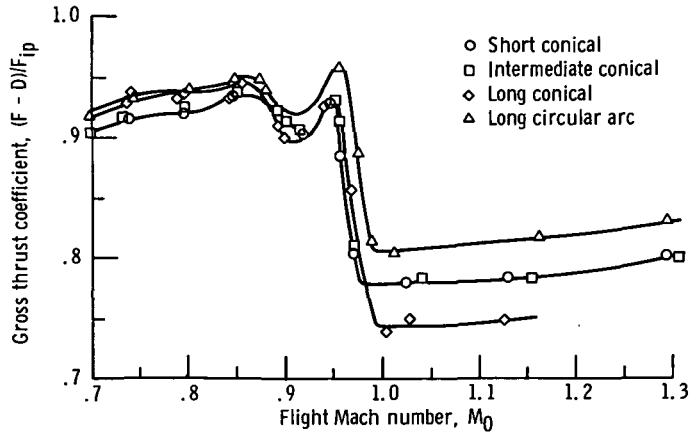

Figure 9. - Effect of boattailed primary geometry on plug nozzle performance. Military power; corrected secondary weight flow, $\omega\sqrt{\tau} \approx 0.01$.

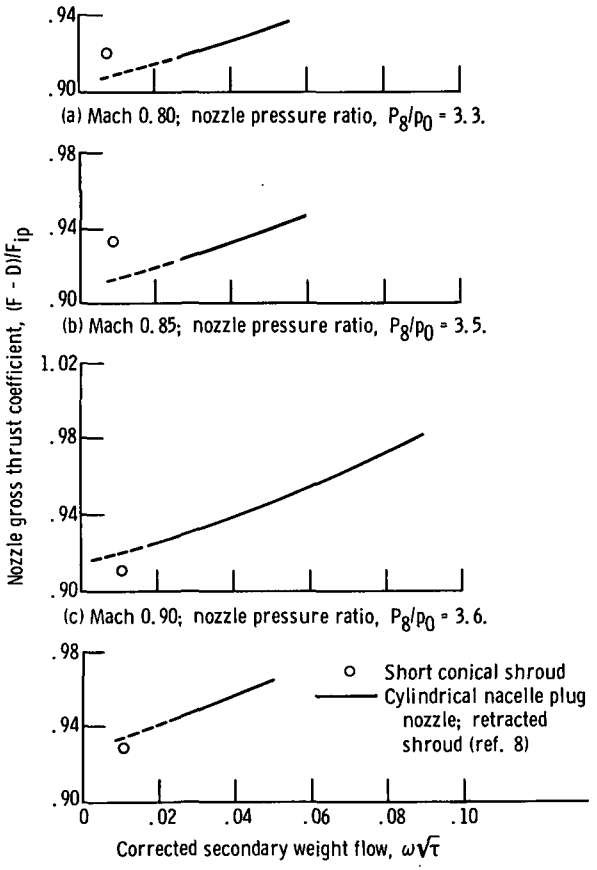

Figure 10. - Comparison of short conical shroud boattailed plug nozzle performance with cylindrical nacelle plug nozzle with 17° conical primary and retracted shroud. Military power.

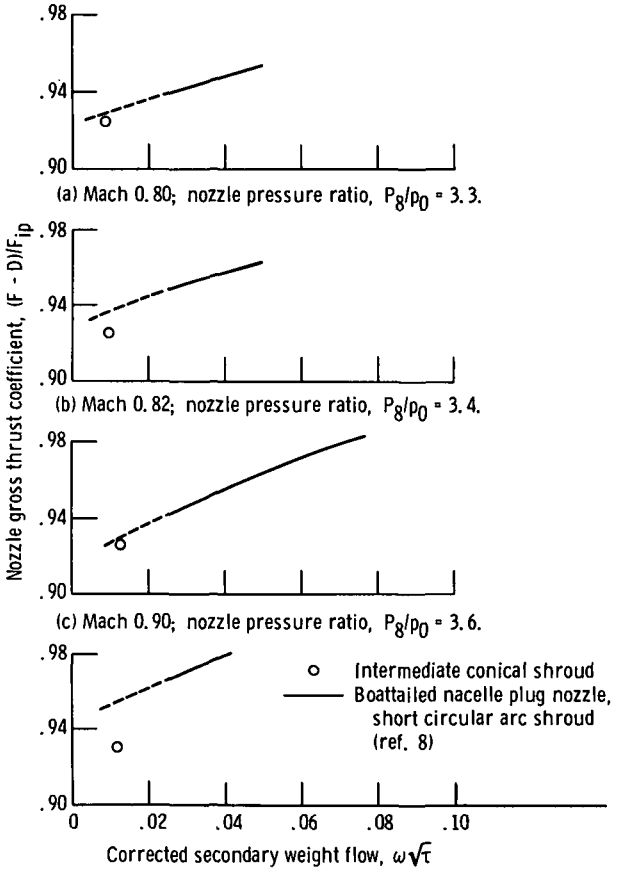

Figure 11. - Comparison of intermediate conical shroud boattailed plug nozzle performance with boattailed nacelle plug nozzle with short circular arc shroud. Military power.

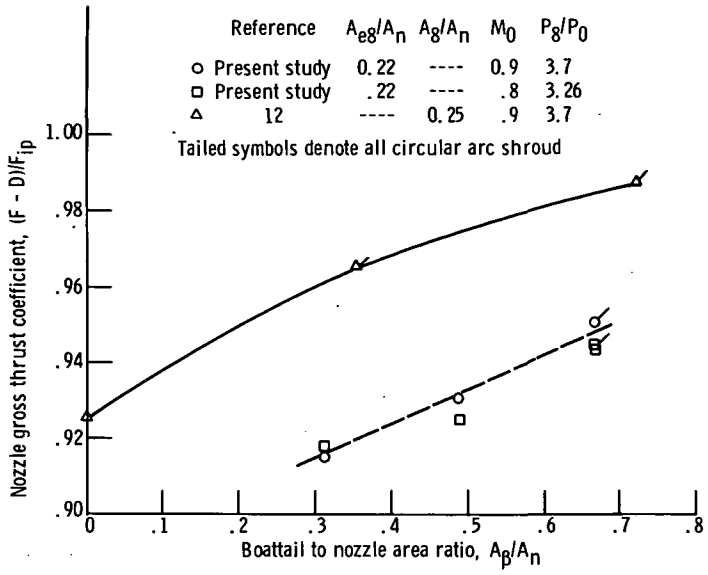

Figure 12. - Effect of boattail projected area on gross thrust coefficient.

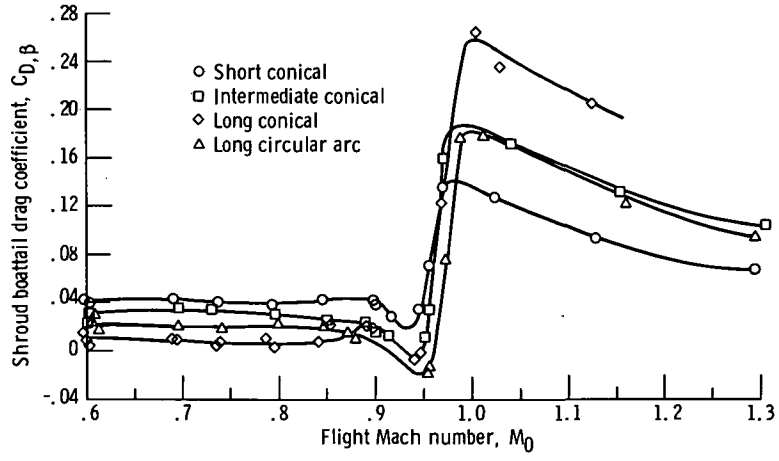

Figure 13. - Variation of pressure drag coefficient with changes in boattailed primary shroud geometry. Military power; corrected secondary weight flow, $\omega\sqrt{\tau} \approx 0.01$.

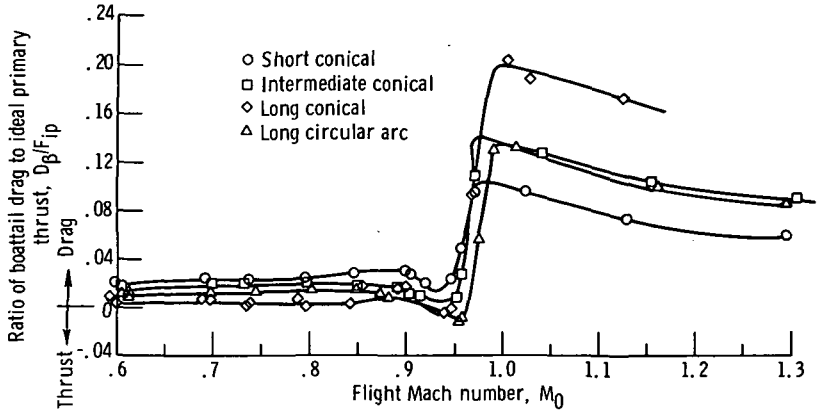

Figure 14. - Effect of boattailed primary shroud geometry on ratio of boattail drag to ideal primary thrust. Military power; corrected secondary weight flow, $\omega\sqrt{\theta} \approx 0.01$.

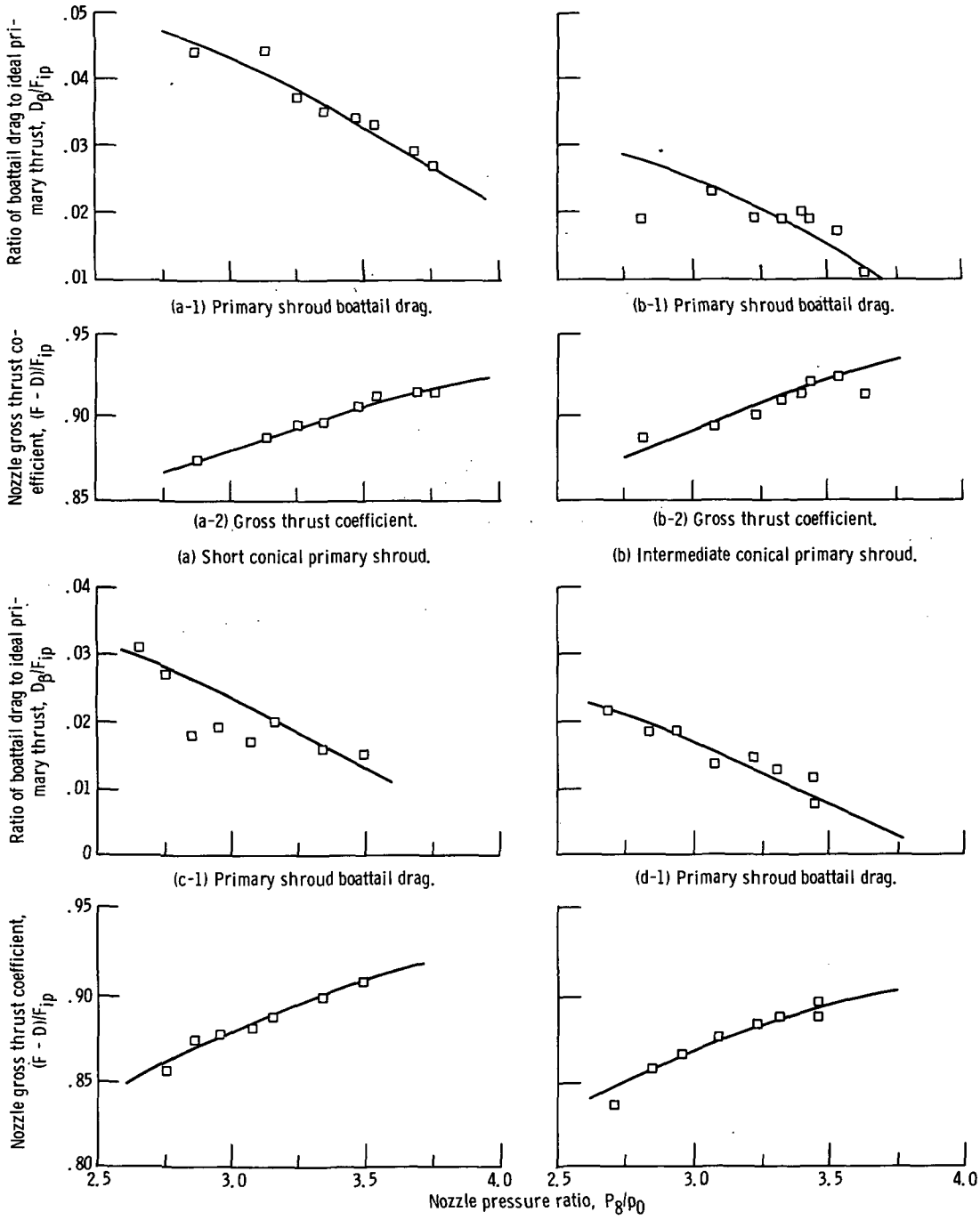

(a-1) Primary shroud boattail drag.

(a-2) Gross thrust coefficient.

(a) Short conical primary shroud.

(b-1) Primary shroud boattail drag.

(b-2) Gross thrust coefficient.

(b) Intermediate conical primary shroud.

(c-1) Primary shroud boattail drag.

(c-2) Gross thrust coefficient.

(c) Long conical primary shroud.

(d-1) Primary shroud boattail drag.

(d-2) Gross thrust coefficient.

(d) Long circular arc primary shroud.

Figure 15. - Effect of nozzle pressure ratio on nozzle gross thrust coefficient and primary shroud drag ratio for Mach 0.9.

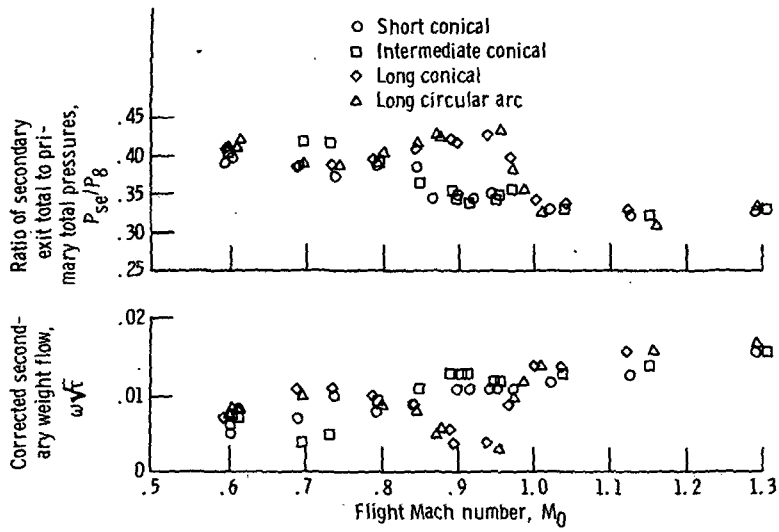

Figure 16. - Nozzle pumping characteristics. Military power.

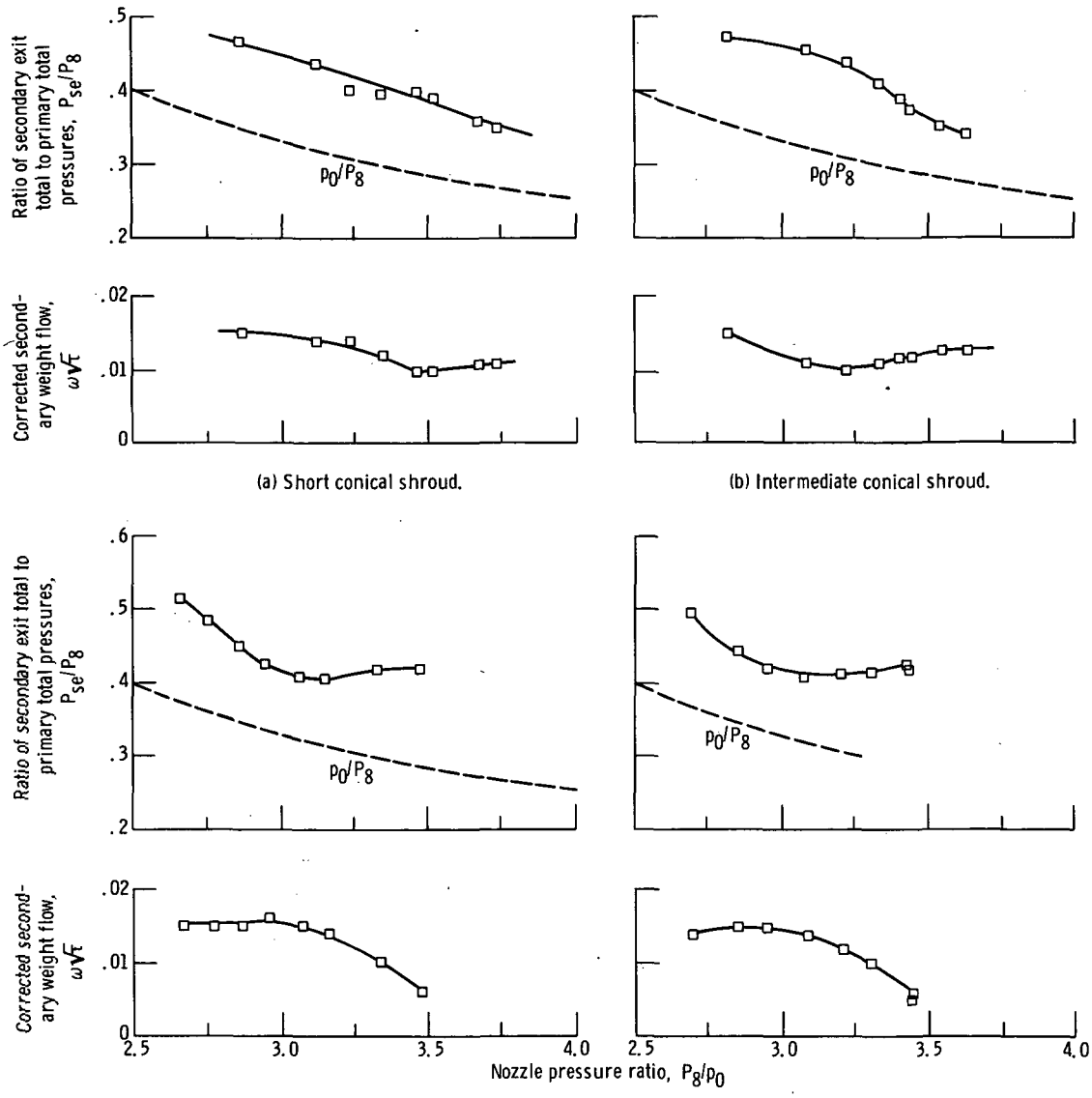

Figure 17. - Effect of pressure ratio on nozzle pumping characteristics for Mach 0.90.

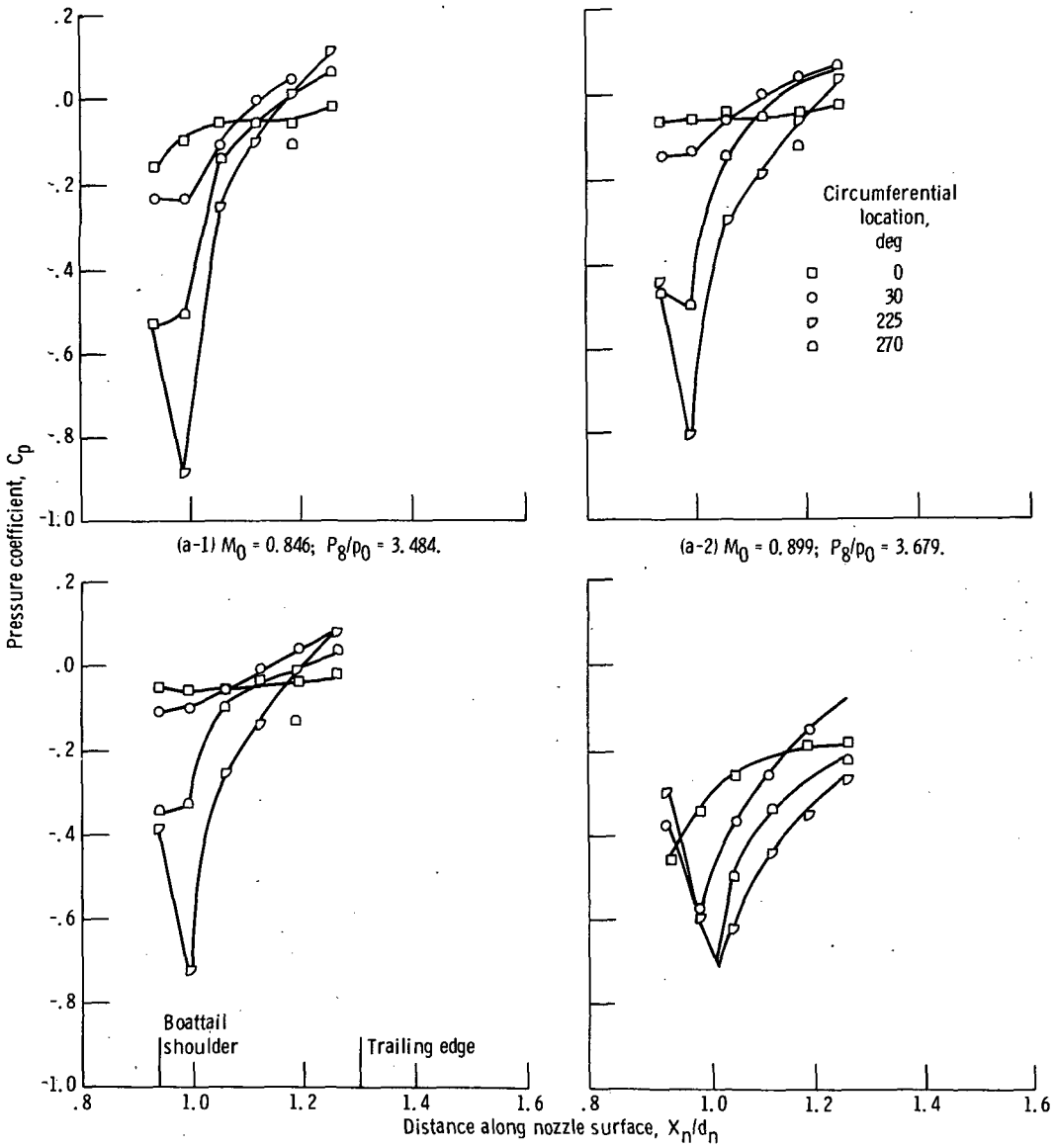

(a-1) $M_0 = 0.846$; $P_8/p_0 = 3.484$.

(a-2) $M_0 = 0.899$; $P_8/p_0 = 3.679$.

(a-3) $M_0 = 0.945$; $P_8/p_0 = 3.939$.

(a-4) $M_0 = 1.023$; $P_8/p_0 = 4.226$.

(a) Short conical primary shroud.

Figure 18. - Effect of installation on boattailed primary shroud pressure distributions. Military power; corrected secondary weight flow, $\omega \sqrt{\tau} \approx 0.01$; flight Mach number, M_0; nozzle pressure ratio, P_8/p_0.

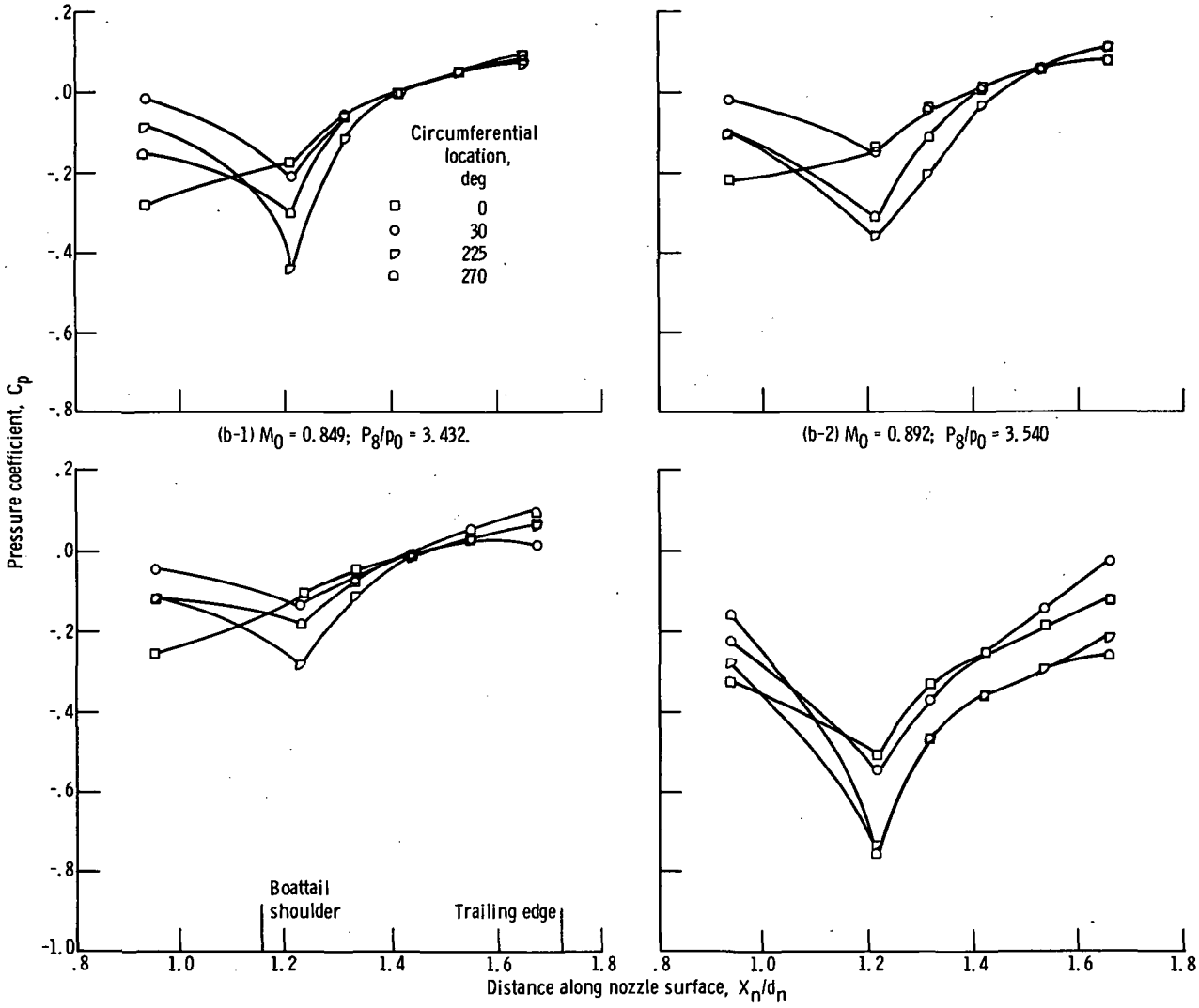

(b-1) $M_0 = 0.849$; $P_8/p_0 = 3.432$.

(b-2) $M_0 = 0.892$; $P_8/p_0 = 3.540$

(b-3) $M_0 = 0.951$; $P_8/p_0 = 3.917$.

(b-4) $M_0 = 1.040$; $P_8/p_0 = 4.240$.

(b) Intermediate conical primary shroud.

Figure 18. - Continued.

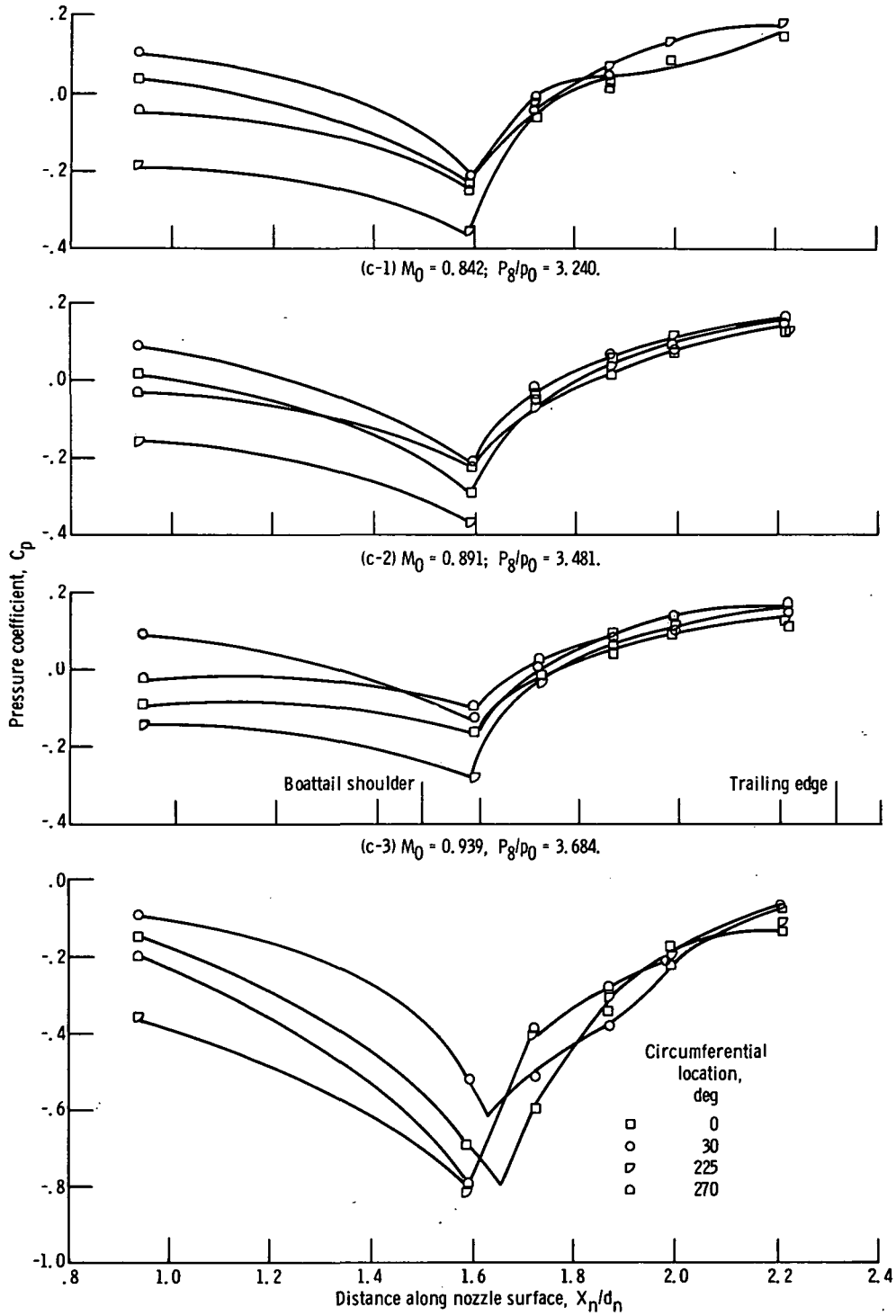

(c-1) $M_0 = 0.842$; $P_8/p_0 = 3.240$.

(c-2) $M_0 = 0.891$; $P_8/p_0 = 3.481$.

(c-3) $M_0 = 0.939$, $P_8/p_0 = 3.684$.

(c-4) $M_0 = 1.003$; $P_8/p_0 = 3.911$.

(c) Long conical primary shroud.

Figure 18. - Continued.

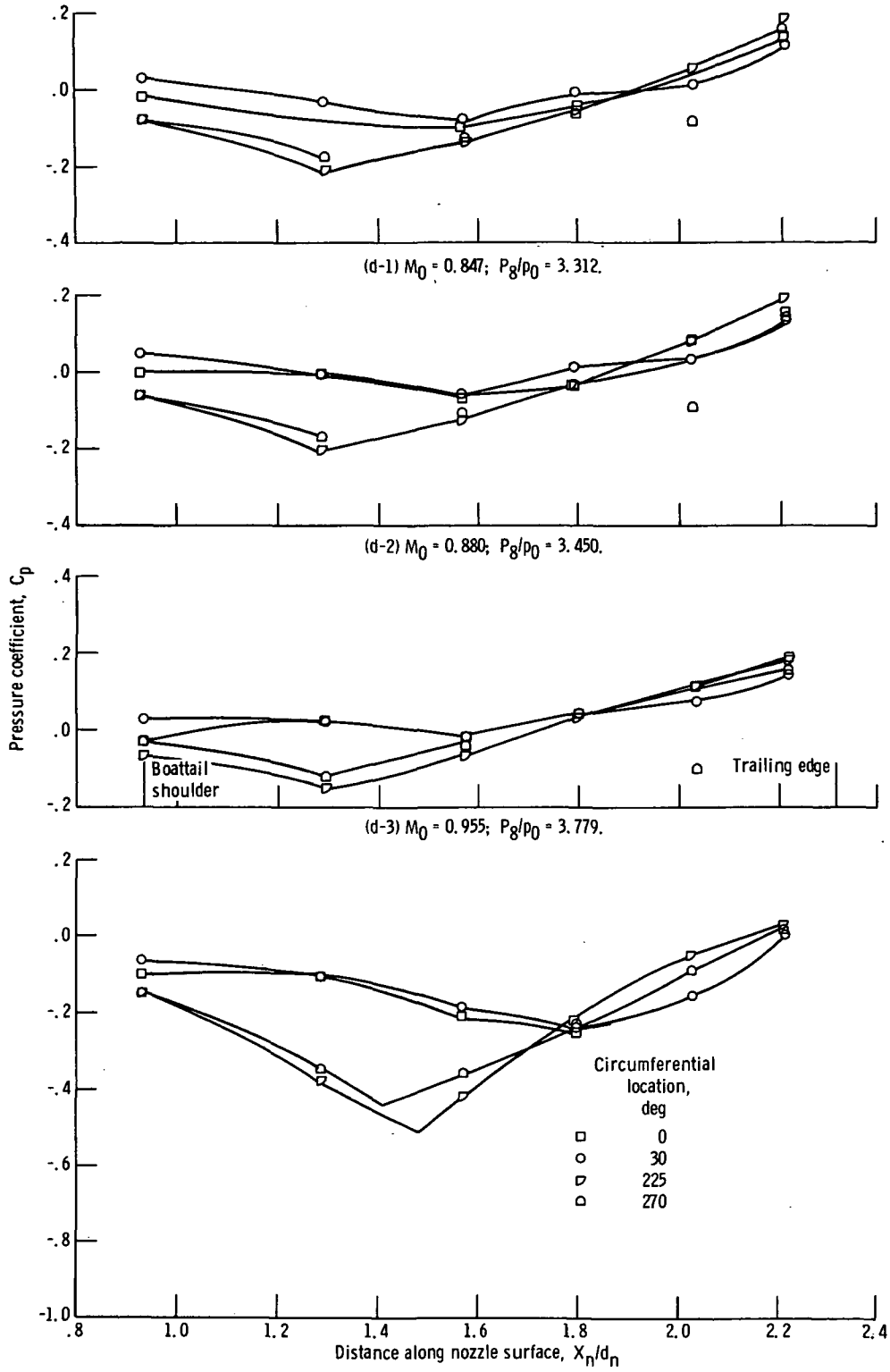

(d) Long circular arc primary shroud.

Figure 18. - Concluded.

"The aeronautical and space activities of the United States shall be conducted so as to contribute . . . to the expansion of human knowledge of phenomena in the atmosphere and space. The Administration shall provide for the widest practicable and appropriate dissemination of information concerning its activities and the results thereof."

—NATIONAL AERONAUTICS AND SPACE ACT OF 1958

NASA SCIENTIFIC AND TECHNICAL PUBLICATIONS

TECHNICAL REPORTS: Scientific and technical information considered important, complete, and a lasting contribution to existing knowledge.

TECHNICAL NOTES: Information less broad in scope but nevertheless of importance as a contribution to existing knowledge.

TECHNICAL MEMORANDUMS: Information receiving limited distribution because of preliminary data, security classification, or other reasons. Also includes conference proceedings with either limited or unlimited distribution.

CONTRACTOR REPORTS: Scientific and technical information generated under a NASA contract or grant and considered an important contribution to existing knowledge.

TECHNICAL TRANSLATIONS: Information published in a foreign language considered to merit NASA distribution in English.

SPECIAL PUBLICATIONS: Information derived from or of value to NASA activities. Publications include final reports of major projects, monographs, data compilations, handbooks, sourcebooks, and special bibliographies.

TECHNOLOGY UTILIZATION PUBLICATIONS: Information on technology used by NASA that may be of particular interest in commercial and other non-aerospace applications. Publications include Tech Briefs, Technology Utilization Reports and Technology Surveys.

Details on the availability of these publications may be obtained from:

SCIENTIFIC AND TECHNICAL INFORMATION OFFICE

NATIONAL AERONAUTICS AND SPACE ADMINISTRATION

Washington, D.C. 20546